Journal of Alloys and Compounds 509 (2011) 2716–2722

Contents lists available at ScienceDirect

Journal of Alloys and Compounds

journal homepage: www.elsevier.com/locate/jallcom

The influence of imposed strain on the development of microstructure and transformation characteristics of Ni–Ti shape memory alloys

Radim Kocich [a,*], Miroslav Kursa [b], Ivo Szurman [b], Antonín Dlouhý [c]

[a] Department of Material Forming, Faculty of Metallurgy and Materials Engineering, VŠB TU Ostrava 17.listopadu 15, 70833 Ostrava-Poruba, Czech Republic
[b] Department of Non Ferrous Metals-Refining and Recycling, Faculty of Metallurgy and Materials Engineering, VŠB TU Ostrava 17.listopadu 15, 70833 Ostrava-Poruba, Czech Republic
[c] Department of Mechanical Properties, Institute of Physics of Materials, Academy of Sciences of the Czech Republic, Žižkova 22, 616 62 Brno, Czech Republic

ARTICLE INFO

Article history:
Received 30 September 2010
Received in revised form
25 November 2010
Accepted 1 December 2010
Available online 7 December 2010

Keywords:
Intermetallics
Metals and alloys
Shape memory
TEM

ABSTRACT

Presented paper describes the influence of imposed strain on the development of microstructure (substructure) in Ni–Ti materials during the application of ECAE (equal channel angular extrusion). The interrelationship between imposed strain and resulting transformation characteristics is in the main point of interest while the chemical composition, namely the occurrence of secondary phases such as TiC and Ti_4Ni_2O resulting from the technology used for the sample alloy preparation is also investigated. The alloy Ni50.6–Ti (at.%) was prepared by melting in the HF vacuum induction furnace using a graphite crucible. The deformation was carried out via ECAE combined with prior rotary forging/swaging. ECAE was carried out at 280 °C. The imposed strain had the value ~2. The alloy was processed by deformation route Bc. It was established the high dislocation density generated by the imposed strain stabilized the B2 and R phases and shifted the transformation R ↔ B19′ towards the lower temperature region. Direct effect of the deformation stress was demonstrated in samples after the second pass when the occurrence of the deformation induced transformation B2 → B19′ was confirmed. Deformation induced transformation also represents contribution to the overall deformation of the samples during the process.

1. Introduction

ECAE represents a very popular severe plastic deformation (SPD) method applied to the metallic materials in order to improve their utility characteristics [1–3]. Introduction of large deformations during this process allows influencing the microstructure of pure metals as well as alloys considerably [4–6]. Particular attention in this field has been paid to the investigation of the alloys based on the light metals Al, Mg [7–9] while relatively limited effort so far has been devoted to the complex alloy systems involving phase transformation or twinning during ECAE processing such as in NiTi [10–12], Ti [13]. Depending on the phase stability, the dominant deformation mechanism in β-titanium alloys can change from dislocation slip to twinning/martensitic transformation [14]. It has been demonstrated the interaction between the mechanisms favorably contributes to the grain size refining process [15,16]. Conventional forming technologies such as cold rolling can also produce nanostructure (grains less than 50 and 100 nm), as it has been confirmed for β-titanium alloys [17]; however, nanostructure produced in this manner is thermally unstable and increase of the temperature above 500 °C brings a rapid grain size growth. Relative microstructure stability of materials manufactured via SPD method justifies attempts to introduce this method on a macro scale. For example, Stolyarov [18,19] combined multi-pass ECAE and cold extrusion/cold rolling processes to produce an alloy-like pure titanium material. In both experiments, a decrease in grain size improved mechanical properties such as yield and tensile strength.

One of the characteristic features of Ni–Ti shape memory alloys is that the martensitic phases R, B19 and B19′ produced by the cooling of the cubic B2 phase display a lower crystalline symmetry than the original B2 phase. Having defined crystallographic relation between the parent phase (B2 austenite) and the product phases (R phases or B19′), the lower symmetry of martensitic crystals can lead to the formation of several crystallographic variants of martensite within one originally austenitic grain. Saburi [20] describes the existence of 4 crystallographically equivalent variants for type R martensite, 6 variants of B19 martensite and 12 variants for type B19′ martensite. The crystallographic relation between the original austenitic B2 crystal and the B19′ martensite is further complicated by the process of twinning – a mechanism enabling the shape of the martensitic crystal to be accommodated within the austenitic matrix (via lattice invariant shear – LIS) [21]. It has been proved that twinning mechanism in B19′ martensite is of the type II, with the axis in ⟨0 1 1⟩ direction [22,23]. Considering the extensive transfor-

* Corresponding author.
E-mail address: radim.kocich@vsb.cz (R. Kocich).

0925-8388/$ – see front matter © 2010 Elsevier B.V. All rights reserved.
doi:10.1016/j.jallcom.2010.12.003

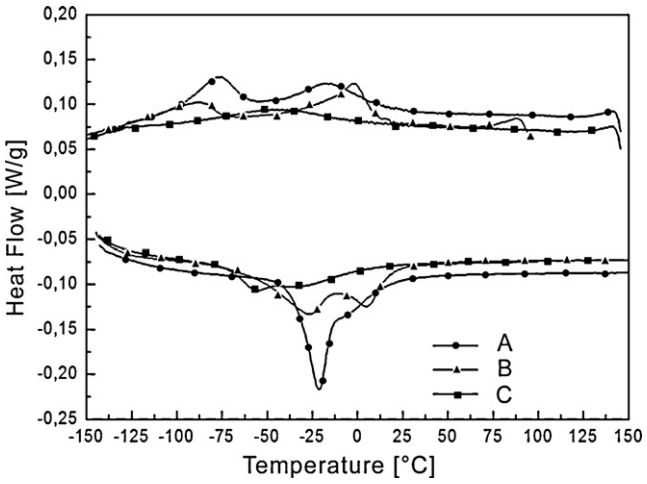

Fig. 1. DSC curves for NiTi samples processed by ECAE.

mation deformation accompanying the phase transition B2 → B19′, the twinning process occurs within each martensitic crystal.

Forming properties of Ni–Ti alloys are strongly dependent on the purity of the manufactured material; the mutual ratio of the two elements plays the key role in the micro structural behavior. Presented study aims to determine the effects of ECAE technology on the development of microstructure (substructure) in Ni–Ti materials. The progress of the transformation characteristics and the influence of imposed strain on transformation paths during ECAE were evaluated and further related to the initial chemical composition.

2. Materials and methods

2.1. Alloy and processing

The alloy Ni50.6–Ti (at.%) was selected for the experiment. The alloy was smelted in a HF vacuum induction furnace using a graphite crucible and casted into graphite form. Rods of diameter 5 mm and length approximately 150 mm were produced using rotary forging. To remove the effects of the prior processing, rods were subsequently submitted to heat treatment (annealing) at 800 °C/30 min. Annealed sample (marked A) was set aside for further analysis. Two samples were produced by extrusion using the ECAE method. In accordance with previous experience [24], two ECAE passes were carried out. The working temperature of the extrusion itself was 280 °C, but the material was pre-heated to a higher temperature before extrusion, namely 500 °C, for a very short time (2 min), in order to prevent heat loss during the handling. The forming method consisted of two passes; the samples for further analysis were set aside after each pass (sample after first pass was marked B, sample after second pass was marked C). The deformation route Bc proved to be suitable namely for the sample C which underwent more than one ECAE pass.

Table 1
Transformation temperatures and enthalpies for samples A, B and C – cooling.

Sample	R_s [°C]	R_p [°C]	R_f [°C]	M_s [°C]	M_p [°C]	M_f [°C]	ΔH [J/g]
A	19	−17	−56	−56	−77	−100	14.6
B	13	−2	−29	−72	−88	−128	16.3
C	–	–	–	7	−42	−99	6.9

Table 2
Transformation temperatures and enthalpies for samples A, B,and C – heating.

Sample	R_{As} [°C]	R_{Ap} [°C]	R_{Af} [°C]	A_s [°C]	A_p [°C]	A_f [°C]	ΔH [J/g]
A	−35	−21	−11	–	−20	−17.5	
B	−64	−26	−4	−26	5	20	−17.9
C	−75	−56	−12	–	−34	11	−11.7

The benchmark composition of the experimental alloy was determined from a surface measuring 30 μm × 20 μm using EDAX SEM analysis (JEOL-JSM-6460 equipped with an INCA Energy analyzer); the Ni content was found to be 50.4 at.% (on average of 3 measurements).

2.2. DSC analysis

Transformation characteristics of the samples A, B,and C were measured using the differential scanning calorimetry (DSC); the released and/or absorbed latent heat associated with martensitic transformations is measured in predetermined transformation temperature as principal of this method. The measurement was carried out using DSC 204 F1 Phoenix/Netzsch equipment which enables for the output correction relative to the signal of an empty sample cell for any number of data points within the studied temperature interval.

Selected heating cycle consisted of several heating/cooling segments. Initially at room temperature, the sample was heated at rate 10 °C/min up to 150 °C and exothermically held for 180 s, followed the cooling period at rate 10 °C/min to -150 °C and a further 180 s isothermic dwell. After that, the sample was heated again at the same rate back up to 150 °C and isothermically held for 180 s, than cooled to the room temperature. The DSC signal gathered during the cooling (150 °C → −150 °C) and heating (−150 °C → 150 °C) cycles was consequently analyzed.

2.3. SEM analysis

The grain size was evaluated on thin films using SEM. It should be noted observed grain size was in range not detectable by standard metallographic methods including light microscopy and/or SEM performed on bulk metallographic samples.

2.4. TEM analysis

Preparation of thin films from TiNi samples requires some additional attention with respect to preservation of the original microstructure. It is important to ensure sufficient heat transfer from the samples and also to control applied mechanical

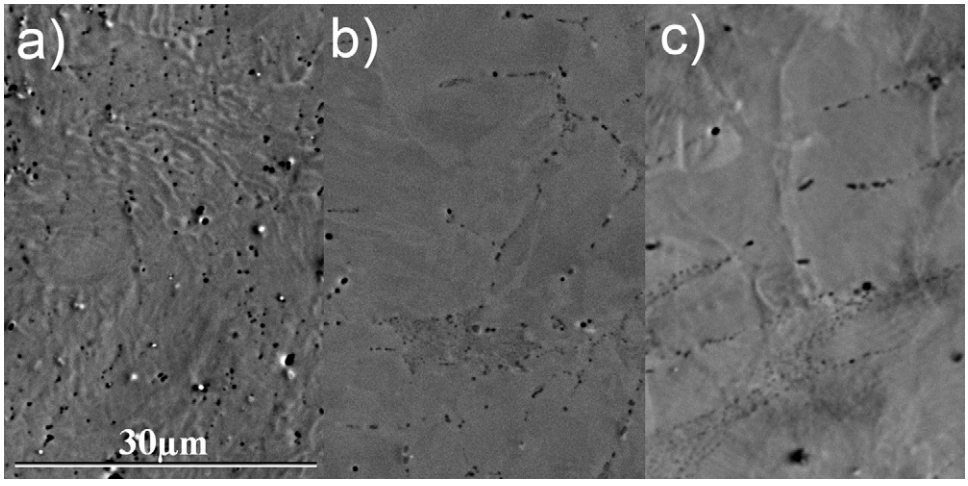

Fig. 2. SEM images of processed samples.

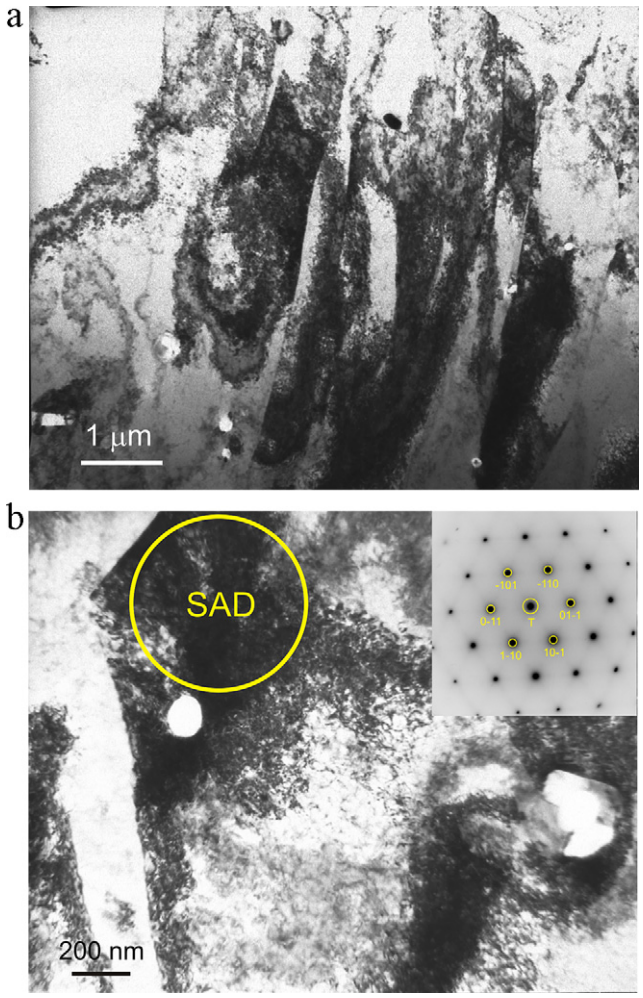

Fig. 3. (a) TEM image of sample A – dislocation boundaries after rotary forging and subsequent heat treatment (800 °C/30 min).(b) TEM – bright field with shutter position marking and corresponding SAD – zone $\langle 1\,1\,1\rangle_{B2}$ in sample A after rotary forging and following heat treatment (800 °C/30 min), high dislocation density (4.3×10^{14} m^{-2}).

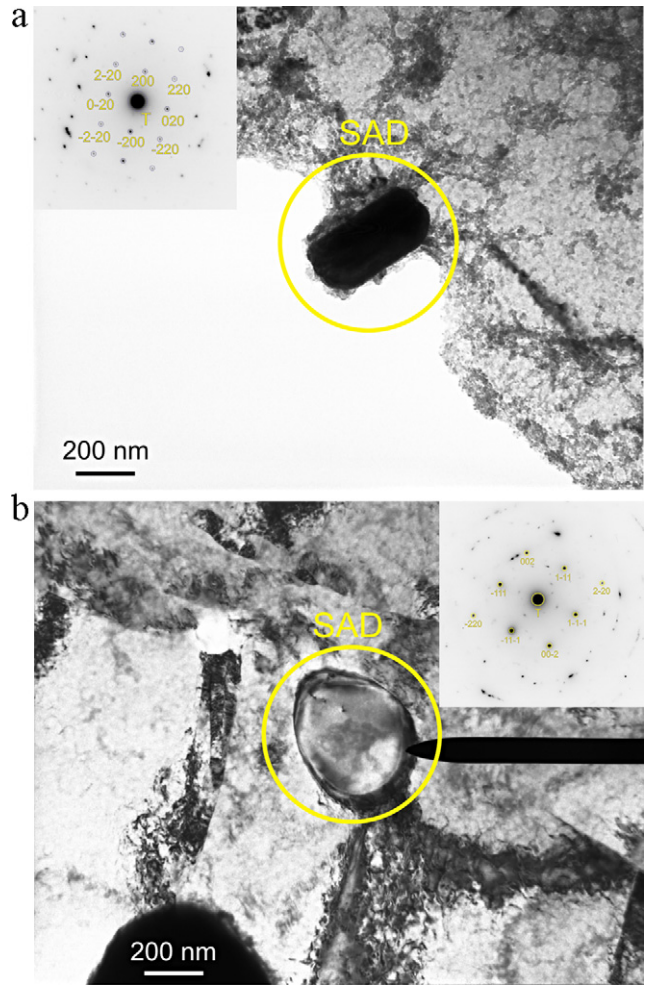

Fig. 4. (a) Oxidic particle Ti_4Ni_2O in sample A – TEM image, corresponding SAD – zone $\langle 0\,0\,1\rangle_{Ti_4Ni_2O}$. (b) TEM diffraction analysis of TiC particle in sample A, corresponding SAD – zone $\langle 110\rangle_{TiC}$.

stress during the preparation process in order to prevent initiation of the stress induced phase transformations. Samples for TEM were cut from the bulk material using electric spark cutter in direction perpendicular to the rod axis, cut segments were mechanically ground and further electrolytically thinned. Thinning was carried out in the solution of 95% CH_3COOH + 5% $HClO_4$, at 60 V and in controlled temperature environment above +10 °C.

Dislocation density was measured in accordance with Ham [25]; the thin film thickness was estimated using stereo photography method [26]. It was utilized that TEM enables to combine the morphological information gained from the image formed in a light or dark field with the information from the diffraction images produced via selected area diffraction (SAD) or convergent beam electron diffraction (CBED). Thus the mutual disorientation (mutual rotation angle of crystal lattices) of individual micro structural components (grains, dislocation cells) was characterized using the CBED method [27].

3. Results

3.1. DSC analysis

The characteristic temperatures of transformations (B2 → R, R → B19′ and B19′ → B2) deduced from the DSC curves for all samples are summarized in Table 1 and 2 (cooling and heating respectively). The charts of DSC curves for all studied samples are shown in Fig. 1.

Generally, it can be expected that the DSC curve capturing martensitic transformation B2 → B19′ of the heat treated sample with the Ni content higher than 50.5 at.% would exhibit two steps during the cooling process, including the formation of rhomboedric R phase [19]: B2 → R and R → B19′.

However, the two-step transformation manner was observed only in the case of samples A and B as it is demonstrated by the DSC curves (Fig. 1) and summarized in Table 1. The DSC curves attributed to the samples A and B embody two strong peaks corresponding with the partition of the transformation into the two above-mentioned stages. The DSC curves attributed to the sample C (previously subjected to two ECAE cycles) exhibits just one weak transformation stage, which is apparent in relatively wide temperature interval from 7 to −99 °C. While the transformation enthalpies of the complete transformation B2 → B19′ are comparable for samples A and B and attain values of approximately 15 J g^{-1}, the total enthalpy of the exothermic process in sample C reaches only about a half of that value. Possible explanation of observed results can include the assumption that B2 → B19′ transformation was partially suppressed in the portion of the sample C. Such behavior can be a consequence of the stabilization of the B2 or R phases due to a dense dislocation structure and/or the presence of the residual B19′ martensite after the second ECAE cycle.

The influence of dislocation structure on the stability of the B2 phase is also suggested by other features of the DSC curves of samples A and B. Considering the nominal composition of the studied alloy (50.6 at.%), the temperature area of the R → B19′ transformation was expected to range between −10 and −30 °C [28]. However,

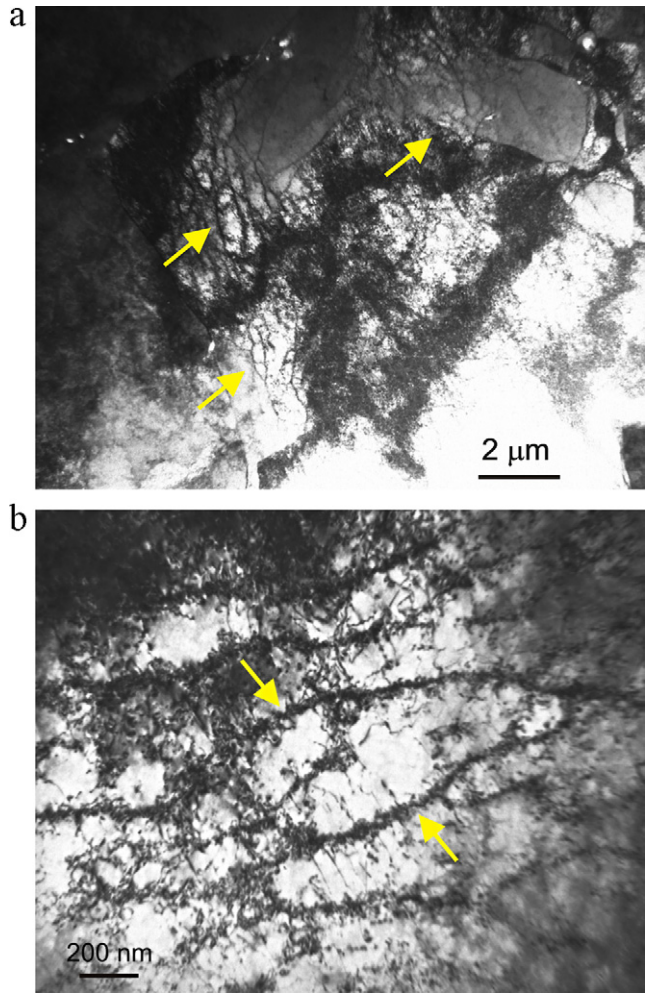

Fig. 5. (a) Dislocation cells in microstructure of sample B after ECAE (1 pass) – TEM image. (b) Detail of dislocation walls in sample B after ECAE (1 pass) – dislocation density ~4.9×10^{14} m^{-2}.

these transformation temperatures were not observed in any case of the studied samples. The values presented in Table 2 demonstrate the temperature of the R → B19′ transformation has fallen into considerably lower region in all three cases. Comparison of the results obtained for samples A and B also suggests that the increase of imposed strain with each additional ECAE pass is accompanied by a continuous decrease of the temperature area for the transformation R → B19′. This observed trend is in accordance with the conclusions reported by Morawiec et al. [29–31], where it was established that increasing degree of deformation (with increasing dislocation density) is accompanied by decrease in transformation temperature. The results obtained from the DSC images of reverse transformation (during heating) are also in accordance with the above mentioned interpretation. Results presented in Table 2 demonstrate the fact increasing ECAE deformation is accompanied with a significant shift of the reverse transformation (R → B19′) temperatures towards lower values. This again corresponds with the process of the stabilization of R phase (destabilization of phase B19′) as a consequence of the high dislocation density.

3.2. SEM analysis

Experimental results for an individual samples are presented in Fig. 2 (sample A – Fig. 2a, sample B – Fig. 2b,and sample C – Fig. 2c). Presented SEM images were produced using back-scattered electrons (BSE), therefore more subtle contrasts corresponding with diffraction on slightly disoriented dislocation cells within the grains are revealed. The images well document that as the number of ECAE cycles increases, the dislocation density accompanied by the decrease in size of the dislocation cells increase.

3.3. TEM analysis

3.3.1. Sample A

Quite unexpected result of TEM observation is the fact that the microstructure of the alloy after rotary forging and heat treatment at 800 °C (prior to the ECAE procedure) has already a relatively high dislocation density. This is visible in Fig. 3a, which is representing the microstructure after intensive deformation (rotary forging); the microstructure has been only partially modified by the subsequent heating to 800 °C. In addition to high dislocation density, Fig. 3a also shows the presence of numerous boundaries which may attributed to the initiation of slip bands during the rotary forging. The dislocation density was determined using images produced at higher magnification. The total dislocation density for sample A can be estimated at 4.3×10^{14} m^{-2} (Fig. 3b). The area specified by the circle on the TEM image indicates the area covered by the selected area diffraction (SAD) determining the particular phase composition of sample A; the axis of depicted zone is $\langle 1\,1\,1 \rangle_{B2}$ (Fig. 3b). The fact that the SAD pattern contains only diffraction traces of the austenitic B2

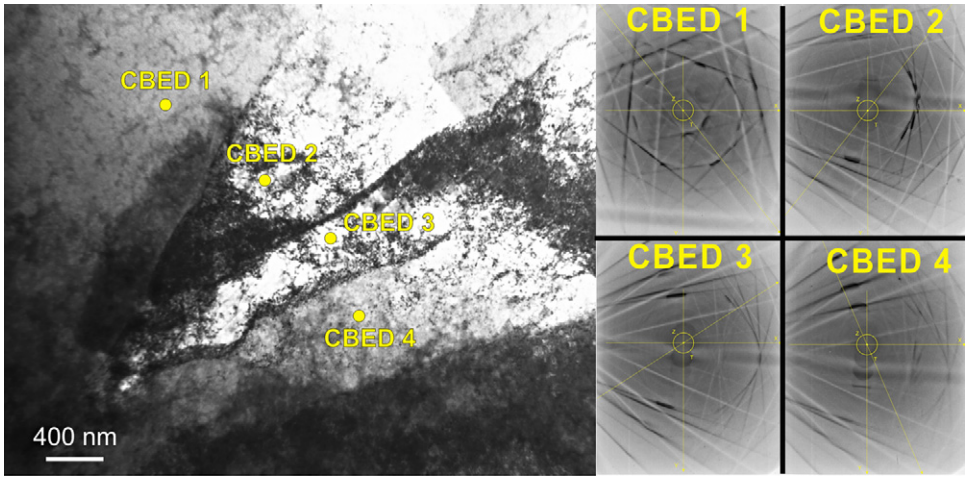

Fig. 6. Crystal lattices misorientation in neighboring dislocation cells of B2 austenite – sample B after ECAE (1 pass). CBED analyses in marked positions.

Table 3
Chemical composition of secondary phases present at Ni–Ti processed by ECAE.

Phase	Ni [at.%]	Ti [at.%]	O [at.%]	C [at.%]
Matrix	50.4	49.6	–	–
Ti_4Ni_2O	33.1	61.5	5.4	–
TiC	0.3	42.9	–	56.8

phase indicates that the original composition of the alloy prior to ECAE the material consisted mainly of austenite without a major presence of phases Ni_4Ti_3, R or B19′.

However, relatively large number of secondary phase particles was detected in the microstructure of sample A (in state prior to ECAE), these particles are most likely a products of metallurgical processes during the preparation. Diffraction analysis of a typical oxide particle Ti_4Ni_2O is presented in Fig. 4a, showing the TEM image of the particle in a light field with marked shutter position and the corresponding diffraction image in the zone axis $[0\,0\,1]_{Ti_4Ni_2O}$. The microstructure contained also TiC carbides, as it is documented by the results of SAD analysis in Fig. 4b; this figure also shows the TEM image with marked shutter position in the zone axis $[1\,1\,0]_{TiC}$. In addition to the diffraction method (SAD), the EDAX method was used for the purposes of the secondary phase identification, providing information on the chemical composition of matrix B2 and the phases produced during the preparation and heat treatment. The results of EDAX analysis in STEM mode are presented in Table 3 (composition of B2 matrix and composition of secondary phases respectively).

3.3.2. Sample B

The main difference between the sample in the initial state (sample A) and the microstructure observed in the samples subjected to ECAE (samples B and C) is the presence of dislocation cells and walls in the latter. Fig. 5a shows TEM images of dislocation cells and extended dislocation walls in sample B after one ECAE cycle. The initiation of dislocation boundaries separating individual cells can ascribed to the intensive deformation during ECAE. The detailed images of dislocation boundaries in Fig. 5b show that dislocations on the boundaries are not arranged into regular networks typical for sub-grain boundary structure. Thus, it can be surmised, the cell boundaries were initiated during deformation at relatively low temperatures, which means it occurred during ECAE. Although it is very difficult to exactly determine the dislocation density on the cell boundaries, it is possible, based on the detailed images of the microstructure of sample B, to estimate the total dislocation density as 4.9×10^{14} m^{-2}. This value represents only a slight increase compared to the initial state; however, detection of dislocation cells as such represents a qualitatively new element in the microstructure after ECAE.

The sequence of TEM images after one pass (Fig. 6) represents an example of the measurement of the mutual misorientation of lattices in the individual dislocation cells. The TEM image in Fig. 6 (in a light field) shows four areas of the microstructure separated by dislocation boundaries. At the marked point within each area, CBED measurement of the orientation of crystal lattices was carried out. The corresponding diffraction images are presented also in Fig. 6. Following quantitative analysis showed that the boundary between cells 1–2 displays a relatively high misorientation angle of 13.2°. The other two are low-angle boundaries with neighboring lattice rotation angles of 3.0° (boundaries 2 and 3) and of 1.4° (boundaries 3 and 4). It was established, based on described results and in accordance with [32], a hierarchical system of dislocation boundaries with varying disorientation angles of neighboring crystallites is produced during the ECAE.

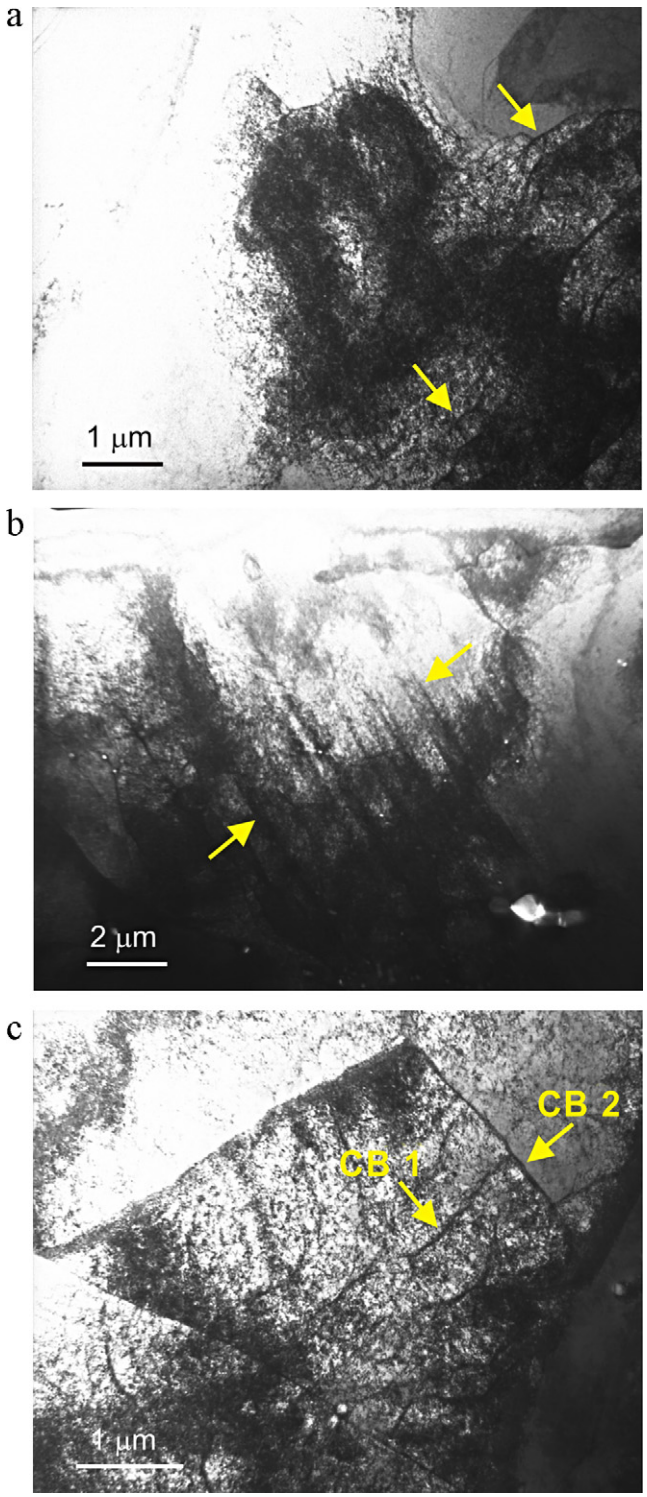

Fig. 7. TEM images of sample C – microstructure after ECAE (2 pass).(a) Dislocation cells.(b) Slip bands.(c) Hierarchy system of dislocation boundaries in sample B after ECAE (2 pass). CB1 – cell boundaries with lower misorientation angleand CB2 – cell boundaries with higher misorientation angle.

3.3.3. Sample C

A strong tendency towards the formation of dislocation cells was also observed in sample C after two ECAE passes. In addition to dislocation cells (Fig. 7a), slip bands are also present in the microstructure (Fig. 7b). Image in Fig. 7c, taken at higher magnification, suggests that the dislocation boundaries form a hierarchical systems. The individual cell boundaries (CB1) merge to

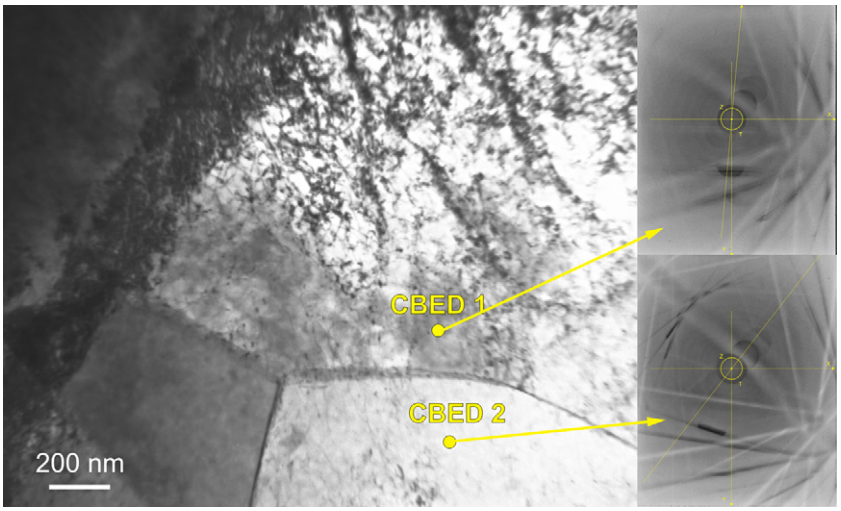

Fig. 8. Crystal lattices misorientation in neighboring dislocation cells of B2 austenite in sample C after ECAE (2 pass). CBED analyses in marked positions

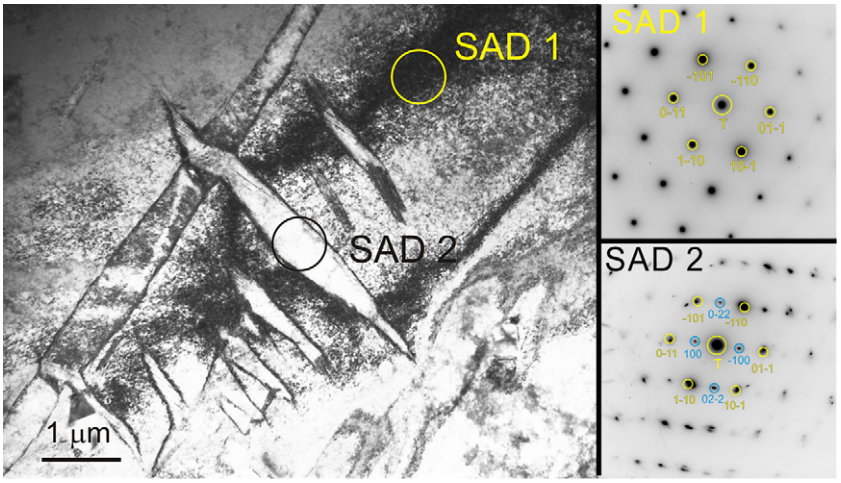

Fig. 9. TEM diffraction analysis of residual austenite B19′ in sample C after ECAE (2 pass). SAD 1 – zone $[1\,1\,1]_{B2}$ and SAD 2 – zone $[0\,1\,1]_{B19'}$.

the dislocation boundaries (CB2) characterized by a higher angle of disorientation of neighboring parts of the B2 austenitic matrix. Comparing microstructure with the state of the sample after one ECAE pass, estimated dislocation density is slightly higher in the sample after two passes, reaching the value of 5.3×10^{14} m^{-2}.

The sequence of TEM images after two passes (Fig. 8) documents the evaluation process of the misorientation in areas of the austenitic B2 matrix separated by a dislocation boundary. The diffraction images (depicted in Fig. 8) were taken from the marked positions on the TEM image (CBED 1, 2). Results of the quantitative assessment show that observed dislocation wall is produced by the rotation of the neighboring lattices of the B2 phase by angle of 6.8°. Such characteristics determine the type of observed boundary as transition between a random incidental boundary [32] and a high angle boundary (HAGB).

Critical stress for the formation of the B19′ phase was reached in several parts of the microstructure [20] due to intensive deformation occurring during the second ECAE pass, resulting from strengthening effect of high dislocation density. Thus, the transformation B2 → B19′ caused by mechanical stress contributes to the deformation of the alloy during ECAE, and residual martensite can be observed in the microstructure after the completion of the process. The TEM images in Fig. 9 document the occurrence of martensite in sample C after the second ECAE pass. The individual martensite crystals are shown also in Fig. 9, together with the specific areas marking the SAD analysis spots. The corresponding diffraction images are presented in SAD 1 (B2 matrix) and SAD 2 (B19′ martensite).

4. Conclusions

Based on the presented experimental results obtained using DSC, SEM and TEM methods, the following conclusions can be formulated for analyzed samples of binary alloy Ti–50.6 at.% Ni:

(1) Relatively high dislocation density, estimated at value 4.3×10^{14} m^{-2}, was observed already in the samples after the preparation and heat treatment of the alloy (prior to ECAE). Such dislocation density values represent the upper limit of detectability using the TEM method.
(2) Two main types of secondary phase particles were detected in the sample alloy after the metallurgical preparation: (i) Ti_4Ni_2O oxidesand (ii) TiC carbides.
(3) Estimated dislocation density raised slightly with increasing numbers of ECAE cycles, up to 5.3×10^{14} m^{-2}. After the first and second cycle, incidental dislocation boundaries were detected separating individual dislocation cells. These were evaluated as low-angle boundaries with misorientation angles of neighbor-

ing cells up to 3°. However, it should not be completely ruled out that the first and second cycle of ECAE also produce hierarchically significant boundaries with higher rotation angles of neighboring crystal lattices.

(4) Deformation stress initiated during the second ECAE cycle was likely to be sufficient enough to stress-induce B2 → B19′ transformation contributing to the total deformation of the sample during the process.

(5) The characteristics of the phase transformations B2 ↔ R ↔ B19′ in sample TiNi alloy determined using above described DSC method were in agreement with the observed state and evolution of the microstructure. High dislocation density had stabilizing effect on both R and B2 phases and the R ↔ B19′ transformation temperature was shifted towards lower values, while this effect became more prominent with an increasing number of ECAE cycles. Observed phase transformation had single step character within relatively wide temperature range after the second ECAE cycle.

Acknowledgements

The presented results were obtained as part of the research project MSM 6198910013 'Processes of preparation and properties of high-purity and structurally defined special materials' and the grant project GA 106/09/1573 'Optimization of chemical composition, structural characteristics, mechanical properties of NiTi alloys for bio-mechanical applications'.

References

[1] V.M. Segal, Materials processing by simple shear, Mater. Sci. Eng. A 197 (1995) 157–164.
[2] R.Z. Valiev, R.K. Islamgaliev, I.V. Alexandrov, Bulk nanostructured materials from severe plastic deformation, Prog. Mater. Sci. 45 (2000) 103–189.
[3] V.M. Segal, Engineering and commercialization of equal channel angular extrusion (ECAE), Mater. Sci. Eng. A 386 (2004) 269–276.
[4] Y. Iwahashi, Z. Horita, M. Nemoto, T.G. Langdon, The process of grain refinement in equal-channel angular pressing, Acta Mater. 46 (1998) 3317–3331.
[5] A.P. Zhilyaev, D.L. Swisher, K. Oh-ishi, T.G. Langdon, T.R. McNelley, Microtexture and microstructure evolution during processing of pure aluminum by repetitive ECAP, Mater. Sci. Eng. A 429 (2006) 137–148.
[6] I. Mazurina, T. Sakai, H. Miura, O. Sitdikov, R. Kaibyshev, Grain refinement in aluminum alloy 2219 during ECAP at 250 °C, Mater. Sci. Eng. A 473 (2008) 297–305.
[7] N.Q. Chinh, J. Gubicza, T. Czeppe, J. Lendvai, Ch. Xu, R.Z. Valiev, T.G. Langdon, Developing a strategy for the processing of age-hardenable alloys by ECAP at room temperature, Mater. Sci. Eng. A 516 (2009) 248–252.
[8] A. Ma, J. Jiang, N. Saito, I. Shigematsu, Y. Yuan, D. Yang, Y. Nishida, Improving both strength and ductility of a Mg alloy through a large number of ECAP passes, Mater. Sci. Eng. A 513–514 (2009) 122–127.
[9] W.J. Kim, C.S. Chung, D.S. Ma, S.I. Hong, H.K. Kim, Optimization of strength and ductility of 2024 Al by equal channel angular pressing (ECAP) and post-ECAP aging, Scr. Mater. 49 (2003) 333–338.
[10] I. Karaman, H.E. Karaca, H.J. Maier, Z.P. Luo, The effect of severe marforming on shape memory characteristics of a Ti-rich NiTi alloy processed using equal channel angular extrusion, Metall. Mater. Trans. A 34 (2003) 2527–2532.
[11] I. Karaman, A.V. Kulkarn, Z.P. Luo, Transformation behaviour and unusual twinning in a NiTi shape memory alloy ausformed using equal channel angular extrusion, Phil. Mag. 85 (2005) 1729–1786.
[12] Ch. Grossmann, J. Frenzel, V. Sampath, T. Depka, G. Eggeler, Elementary transformation and deformation processes and the cyclic stability of NiTi and NiTiCu shape memory spring actuators, Metall. Mater. Trans. 40A (2009) 2530–2544.
[13] D.H. Shin, I. Kim, J. Kim, Y.S. Kim, S.L. Semiatin, Microstructure development during equal-channel angular pressing of titanium, Acta Mater. 51 (2003) 983–996.
[14] T.W. Duerig, J. Albrecht, D. Richter, P. Fischer, Formation and reversion of stress induced martensite in Ti–10V–2Fe–3Al, Acta Metall. 30 (1982) 2161–2172.
[15] K. Wang, N.R. Tao, G. Liu, J. Lu, K. Lu, Plastic strain-induced grain refinement at the nanometer scale in copper, Acta Mater. 54 (2006) 5281–5291.
[16] L. Balogh, T. Ungar, Y. Zhao, Y.T. Zhu, Z. Horita, C. Xu, T.G. Langdon, Influence of stacking-fault energy on microstructural characteristics of ultrafine-grain copper and copper–zinc alloys, Acta Mater. 56 (2008) 809–820.
[17] S.J. Li, Y.W. Zhang, B.B. Sun, Y.L. Hao, R. Yang, Thermal stability and mechanical properties of nanostructured Ti–24Nb–4Zr–7.9Sn alloy, Mater. Sci. Eng. A 480 (2008) 101–108.
[18] V.V. Stolyarov, Y.T. Zhu, T.C. Lowe, R.Z. Valiev, Microstructure and properties of pure Ti processed by ECAP and cold extrusion, Mater. Sci. Eng. A 303 (2001) 82–89.
[19] V.V. Stolyarov, Y.T. Zhu, I.V. Alexandrov, T.C. Lowe, R.Z. Valiev, Grain refinement and properties of pure Ti processed by warm ECAP and cold rolling, Mater. Sci. Eng. A 343 (2003) 43–50.
[20] T. Saburi, Ti–Ni shape memory alloys, in: K. Otsuka, C.M. Wayman (Eds.), Shape Memory Materials, Cambridge University Press, 1998, pp. 49–96.
[21] K. Otsuka, C.M. Wayman, Introduction, in: K. Otsuka, C.M. Wayman (Eds.), Shape Memory Materials, Cambridge University Press, 1998, pp. 1–26.
[22] S. Miyazaki, K. Otsuka, C.M. Wayman, The shape memory mechanism associated with the martensitic transformation in Ti–Ni alloys. I. Self-accommodation, Acta Metall. 37 (1989) 1873–1884.
[23] M. Nishida, K. Yamauchi, A.Y. Chiba, Y. Higashi, Proceedings of ICOMAT'92, Monterey, 1993, p. 881.
[24] R. Kocich, I. Szurman, M. Kursa, J. Fiala, Investigation of influence of preparation and heat treatment on deformation behaviour of the alloy NiTi after ECAE, Mater. Sci. Eng. A 512 (2009) 100–104.
[25] R.K. Ham, The determination of dislocation densities in thin films, Phil. Mag. 6 (1961) 1183–1184.
[26] A. Dlouhý, J. Pešička, Estimate of foil thickness by stereomicroscopy technique, Czech. J. Phys. 40 (1990) 539–543.
[27] A. Dronhofer, J. Pešička, A. Dlouhý, G. Eggeler, On the nature of internal interfaces in tempered martensite ferritic steels, Zeitsch. Metall. 94 (2003) 511–515 (in German).
[28] J. Khalil-Allafi, A. Dlouhý, G. Eggeler, Ni_4Ti_3-precipitation during aging of NiTi shape memory alloys and its influence on martensitic phase transformations, Acta Mater. 50 (2002) 4255–4274.
[29] H. Morawiec, D. Stroz, D. Chrobak, Effect of deformation and thermal treatment of NiTi alloy on transition sequence, J. Phys. IV 5 (1995) C2–C205.
[30] H. Morawiec, D. Stroz, T. Goryczka, D. Chrobak, Two-stage martensitic transformation in a deformed and annealed NiTi alloy, Scr. Mater. 35 (1996) 485–490.
[31] D. Chrobak, H. Morawiec, Thermodynamic analysis of the martensitic transformation in plastically deformed NiTi alloy, Scr. Mater. 44 (2001) 725–730.
[32] D.A. Hughes, N. Hansen, D.J. Bammann, Geometrically necessary boundaries, incidental dislocation boundaries and geometrically necessary dislocations, Scr. Mater. 48 (2003) 147–153.